


Article

# Solar-Light-Driven $\text{Ag}_9(\text{SiO}_4)_2\text{NO}_3$ for Efficient Photocatalytic Bactericidal Performance

Malaa M. Taki<sup>1</sup>, Rahman I. Mahdi<sup>1,\*</sup>, Amar Al-Keisy<sup>1</sup>, Mohammed Alsultan<sup>2,\*</sup>, Nabil Janan Al-Bahnam<sup>3</sup>, Wan Haliza Abd. Majid<sup>4</sup> and Gerhard F. Swiegers<sup>5,\*</sup> 

- <sup>1</sup> Nanotechnology and Advanced Material Research Center, University of Technology-Iraq, Baghdad 10066, Iraq; 11814@uotechnology.edu.iq (M.M.T.); amar.h.alkeisy@uotechnology.edu.iq (A.A.-K.)  
<sup>2</sup> Department of Science, Collage of Basic Education, University of Mosul, Mosul 41002, Iraq  
<sup>3</sup> Department of Physics, Collage of Science for Women, University of Baghdad, Baghdad 10071, Iraq; investigationnabiljb\_phys@cs.w.uobaghdad.edu.iq  
<sup>4</sup> Low Dimensional Materials Research Centre, Department of Physics, Faculty of Science, University of Malaya, Kuala Lumpur 50603, Malaysia; q3haliza@um.edu.my  
<sup>5</sup> ARC Centre of Excellence for Electromaterials Science, Intelligent Polymer Research Institute, University of Wollongong, Wollongong, NSW 2522, Australia  
\* Correspondence: rahman.i.mahdi@uotechnology.edu.iq (R.I.M.); mfka287@uowmail.edu.au (M.A.); swiegers@uow.edu.au (G.F.S.)

**Abstract:** Photocatalytic materials are being investigated as effective bactericides due to their superior ability to inactivate a broad range of dangerous microbes. In this study, the following two types of bacteria were employed for bactericidal purposes: Gram-negative *Escherichia coli* (*E. coli*) and Gram-positive *Staphylococcus aureus* (*S. aureus*). The shape, crystal structure, element percentage, and optical properties of  $\text{Ag}_9(\text{SiO}_4)_2\text{NO}_3$  were examined after it was successfully synthesized by a standard mixing and grinding processing route. Bactericidal efficiency was recorded at 100% by the following two types of light sources: solar and simulated light, with initial photocatalyst concentration of 2  $\mu\text{g}/\text{mL}$ , and 97% and 95% of bactericidal activity in ultra-low photocatalyst concentration of 0.2  $\mu\text{g}/\text{mL}$  by solar and simulated light, respectively, after 10 min. The survival rate was studied for 6 min, resulting in 99.8% inhibition at the photocatalyst dose of 2  $\mu\text{g}/\text{mL}$ . The mechanism of bactericidal efficiency was found to be that the photocatalyst has high oxidation potential in the valence band. Consequently, holes play a significant part in bactericidal efficiency.

**Keywords:**  $\text{Ag}_9(\text{SiO}_4)_2\text{NO}_3$ ; bactericidal efficiency; survival rate; photocatalysis; solar light



**Citation:** Taki, M.M.; Mahdi, R.I.; Al-Keisy, A.; Alsultan, M.; Al-Bahnam, N.J.; Majid, W.H.A.; Swiegers, G.F. Solar-Light-Driven  $\text{Ag}_9(\text{SiO}_4)_2\text{NO}_3$  for Efficient Photocatalytic Bactericidal Performance. *J. Compos. Sci.* **2022**, *6*, 108. <https://doi.org/10.3390/jcs6040108>

Academic Editor: Konda Gokuldoss Prashanth

Received: 3 March 2022

Accepted: 30 March 2022

Published: 6 April 2022

**Publisher's Note:** MDPI stays neutral with regard to jurisdictional claims in published maps and institutional affiliations.



**Copyright:** © 2022 by the authors. Licensee MDPI, Basel, Switzerland. This article is an open access article distributed under the terms and conditions of the Creative Commons Attribution (CC BY) license (<https://creativecommons.org/licenses/by/4.0/>).

## 1. Introduction

Pathogenic diseases in water supplies have recently become a serious medical issue. It has resulted in over a million deaths worldwide [1]. Various strategies have been implemented to sterilize water resources, including chemical treatment using chlorine. Nevertheless, such a technique poses a significant risk and contributes to secondary pollution [2–5]. Thus, there is an urgent need to develop environmentally friendly approaches. Photocatalysis has recently been recognized as one of the most efficient technologies for developing bactericidal surfaces capable of effectively and rapidly inactivating bacteria [6–8]. Even though  $\text{TiO}_2$  nanostructures are the most extensively employed in photocatalysis, they are only active when exposed to UV irradiation, which represents only 4% of the sunlight spectrum [9–15]. The development and engineering of novel photocatalytic materials have been the topic of many publications. However, the practical applications of photocatalysis as antibacterial surfaces and liquids are still in development. Among the many photocatalysts, Ag-based photocatalysts are one of the most promising alternatives due to their strong photocatalytic activity and efficient visible light absorption [16]. Silver silicate compounds undergo strongly oxidative reactions [17–19]. They have a deep valence-band site, which means they can direct the degradation of pathogenic walls through photoinduced

holes and hydroxyl radicals, while photoinduced electrons form super oxides. In general, reactive oxygen species (ROS) can degrade pathogens on surfaces or in liquids. However, lipids, proteins, and DNA can be damaged by ROS [20–22]. Nonetheless, silver-based oxide compounds are being largely resisted due to highly photocorrosion materials [23–25]. Silver silicate, on the other hand, decomposes into silver nanoparticles, which are very sensitive to pathogenic diseases [26–28]. Thus, silver silicate compounds are thought to be selectively appropriate for disinfection and sterilization but not for photodegradation of polluting chemicals or water splitting. Furthermore, it is believed that coating face mask tissue with silver silicate will provide excellent disinfection when exposed to sunlight. Our previous work demonstrated that  $\text{Ag}_{10}\text{Si}_4\text{O}_{13}$  exhibits spontaneous electronic polarization due to the distorted tetrahedral unit ( $\text{SiO}_4$ ) configuration [29]. Therefore, silver silicate compounds are expected to improve charge separation, resulting in enhanced photocatalysis performance. Likewise,  $\text{Ag}_9(\text{SiO}_4)_2\text{NO}_3$  exhibits spontaneous electronic polarization and is advantageous due to a narrow band gap [30]. In this work, we present a facile, efficient, cost-effective, and practical way for the green synthesis of  $\text{Ag}_9(\text{SiO}_4)_2\text{NO}_3$  by simply mixing raw salts and grinding them in a moisture environment using an agate mortar. The photocatalytic bactericidal characteristics, crystal formations, and morphologies were systematically investigated.

## 2. Experimental

### 2.1. Synthesis

$\text{Ag}_9(\text{SiO}_4)_2\text{NO}_3$  was prepared by standard mixing and grinding processing route. Typically, 4.5 mmol  $\text{AgNO}_3$  (Sigma-Aldrich Company, St. Louis, MO, USA) and 1 mmol  $\text{Na}_2\text{SiO}_3$  (Sigma-Aldrich Company) were mixed and grounded in an agate mortar for 15 min in a moisture environment until the white mixture turned deep red. The obtained  $\text{Ag}_9(\text{SiO}_4)_2\text{NO}_3$  was washed five times with distiller water and dried inside an oven at  $60^\circ\text{C}$  for 24 h.

### 2.2. Characterization

The crystal structure and phase purity of the compounds were characterized with X-ray diffraction (XRD, GBC, MMA) using  $\text{Cu K}\alpha$  radiation ( $\lambda = 1.5418 \text{ \AA}$ ). Field-emission scanning electron microscopy (FE-SEM, Joule-JSM-7610F) and energy dispersive spectroscopy (EDS, Bruker, XFlash 6-10) were used to analyze the morphology and elemental analyses of the samples. The UV–Vis absorption spectrum was obtained using Shimadzu-3600 UV–Vis spectrophotometer.

### 2.3. Photocatalytic Inactivation Performance

The spread plate method was used to evaluate antibacterial activity. *E. coli* and *S. aureus* were chosen as the indicator bacteria to represent Gram-negative and Gram-positive bacteria, respectively. The prefabricated bacterial suspension was mixed with a solution of  $\text{Ag}_9(\text{SiO}_4)_2\text{NO}_3$  in deionized water (DI). The initial concentration of  $\text{Ag}_9(\text{SiO}_4)_2\text{NO}_3$  was  $2 \mu\text{g/mL}$ , with a final concentration of  $0.2 \mu\text{g/mL}$ , and a bacterial concentration of  $10^5 \text{ cfu/mL}$ . A magnetic stirrer was used to continuously stir the mixed suspensions at room temperature. After 10 min, the samples were cultured in sunlight. Natural sunlight radiated from 10:00 a.m. to 13:00 p.m. on sunny days (sunlight intensity was  $97 \text{ mW/cm}^2$ ). Every 2 min, 50 mL of diluent-mixed suspensions was added to agar plates (Muller Hinton Agar HIMEDIA) and disseminated. Over 24 h, the plates were incubated at  $37^\circ\text{C}$ . The bacterial colonies on the plates were counted to measure bacterial efficiency. The entire experiment was carried out under sterile conditions. The intensity of the light source (300 W xenon short-arc lamp, toption) was  $147 \text{ mW/cm}^2$ . The same method, as indicated above, was performed using simulated light, with 15 cm distance between the simulated light and the sample.

#### 2.4. Photocatalyst Mechanism

Three experiments were conducted in this process. In the first experiment, 10% vol of  $\text{AgNO}_3$  (1 mM) (Sigma-Aldrich Company) was used as an electron scavenger, and 100 mg of  $\text{Ag}_9(\text{SiO}_4)_2\text{NO}_3$  was added to 100 mL of RhB (10 mg/L) (Sigma-Aldrich Company) and stirred for 30 min in the dark. Simulated light was used to photodegrade RhB for 10 min. Secondly, 10% vol of methanol (1 Mm) (Sigma-Aldrich Company) was added as a hole scavenger, followed by the same procedure as above. The third step is repeating the first but without the scavenger. Finally, UV-Vis spectroscopy was used to evaluate the decolorization of RhB.

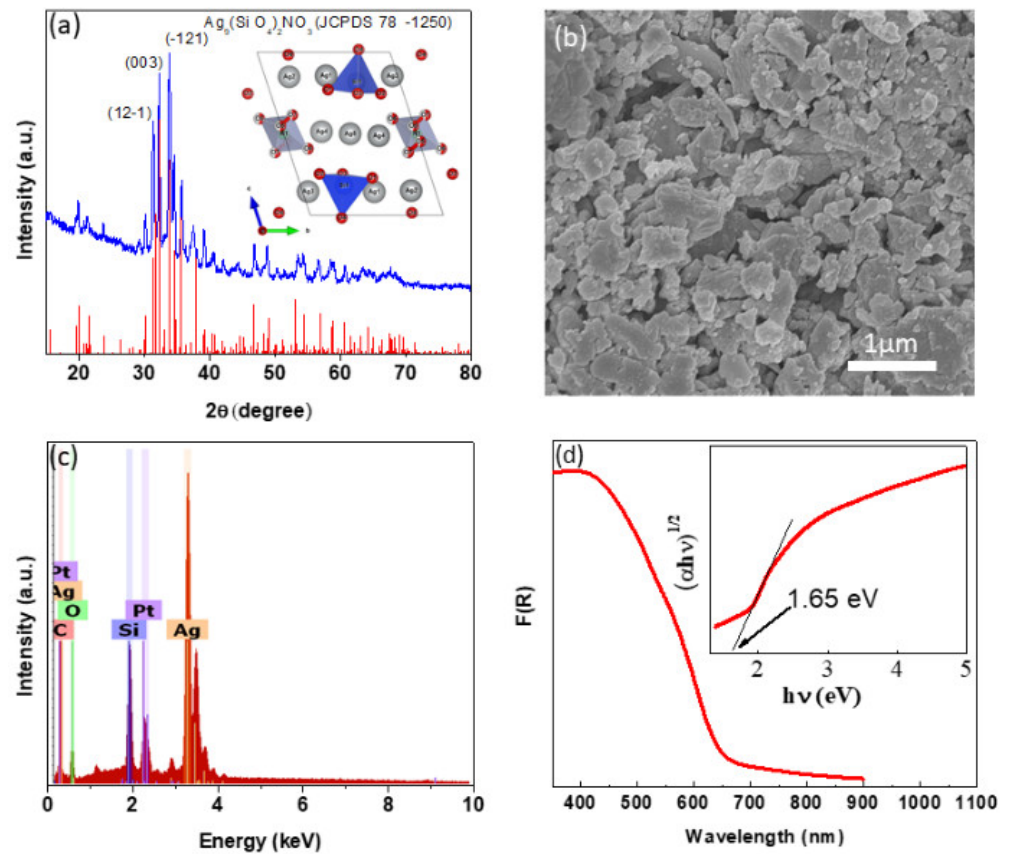
#### 2.5. Calculation

Cambridge Serial Total Energy Package (CASTEP) software was used to implement the first-principle methods [31]. The exchange-correlation interaction was analyzed using the functional method of Perdew–Burke–Ernerhof (GGA-PBE) and the relativistic treatment of Koelling-Harmon. A plane-wave basis with cut-off energy of 500.0000 eV was used as well as a  $3 \times 3 \times 3$  Monkhorst-Pack k-point mesh. The pseudopotential was treated using effective core potential, assuming the system was metallic.

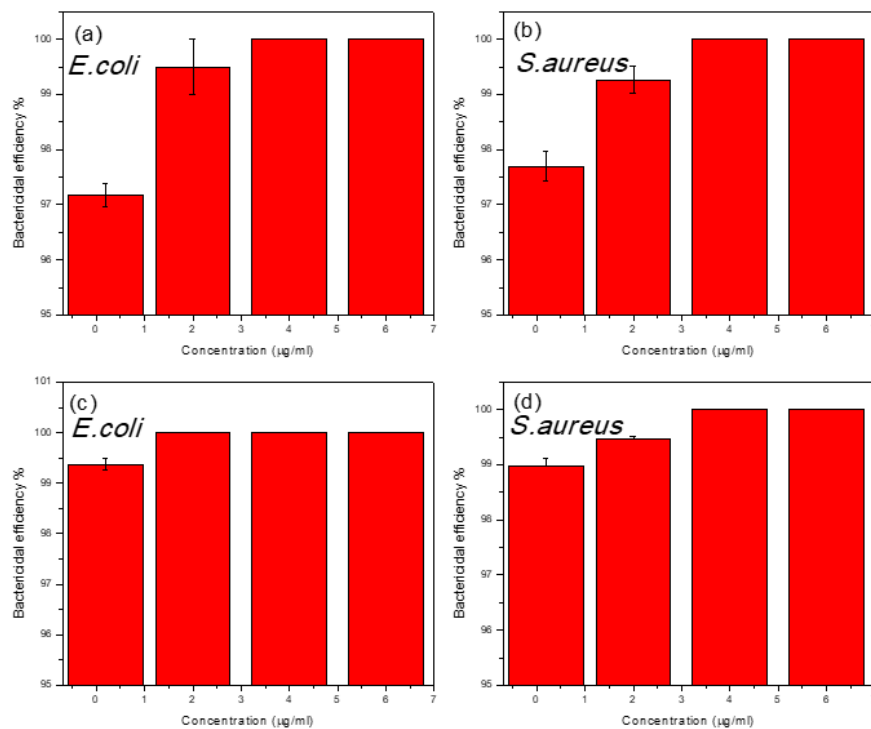
### 3. Results and Discussion

Figure 1a illustrates the powder XRD pattern of the obtained product, which can be classified as the single phase of  $\text{Ag}_9(\text{SiO}_4)_2\text{NO}_3$  (triclinic phase, space group P-1). The most noticeable peaks of  $\text{Ag}_9(\text{SiO}_4)_2\text{NO}_3$  at 31.2, 32.2, and 33.7, which correspond to the planes (12-1), (003), and (-121), respectively, were well matched to the standard pattern (JCPDS card no. 78–1250). There are no signs of impurities, which suggests that high purity  $\text{Ag}_9(\text{SiO}_4)_2\text{NO}_3$  was obtained. The morphology of the  $\text{Ag}_9(\text{SiO}_4)_2\text{NO}_3$  is shown in an FE-SEM image (Figure 1b), which confirmed the particle size in nanoscale and ranged in size from 50 to 200 nm, with irregularly tending to have a sheet-like shape. It should also be noted that several small nanoparticles are seen on the surface of the nanosheets, which are most likely silver nanoparticles formed during SEM characterization by the reduction of  $\text{Ag}^+$  in  $\text{Ag}_9(\text{SiO}_4)_2\text{NO}_3$  under high-energy electron-beam irradiation, which is frequent in Ag–sulfur compounds. To further confirm the purification of the materials, elemental assessment was conducted (Figure 1c). The percentages of each element were 42%, 3.2%, 54%, and 0.8% for Ag, Si, O, and N, respectively, which corresponds with the compound percentage. There was no indication of additional elements, confirming the excellent purity of  $\text{Ag}_9(\text{SiO}_4)_2\text{NO}_3$ . The optical characteristics of the material are presented in Figure 1d. The results clearly show full absorption in the UV-Vis range indicating that the material exhibits excellent optical properties.

As shown in Figure 2, the tested concentrations (*E. coli* and *S. aureus*) have high sensitivity to both simulated and solar light. After repeated dilution, the cell population was estimated by colony counting on agar plates. Both the first two high concentrations of 0.06 and 0.04 mg/mL were found to be 100% effective in killing Gram-positive and Gram-negative bacteria, as shown in Figure 2a–d, under simulated and solar light. There were three separate experiments, each of which was referred to as the “first”, “second”, and “third” attempt; the 2  $\mu\text{g}/\text{mL}$  and 0.2  $\mu\text{g}/\text{mL}$  concentrations had differing bactericidal properties. The bactericidal efficiency of *E. coli* and *S. aureus* was 99% and 97%, respectively, at 2  $\mu\text{g}/\text{mL}$ , whereas at 0.2  $\mu\text{g}/\text{mL}$ , the bactericidal efficiency of *E. coli* and *S. aureus* was 97% and 97.5%, respectively. Solar light appears to be better than simulated light, which may be because it contains the full spectrum of light.



**Figure 1.** (a) XRD pattern and visual crystal structure of Ag<sub>9</sub>(SiO<sub>4</sub>)<sub>2</sub>NO<sub>3</sub>. (b) FE-SEM image. (c) EDX element percentage of Ag<sub>9</sub>(SiO<sub>4</sub>)<sub>2</sub>NO<sub>3</sub>. (d) UV-Vis spectra and inset band-gap measurement of Ag<sub>9</sub>(SiO<sub>4</sub>)<sub>2</sub>NO<sub>3</sub>.



**Figure 2.** The bactericidal efficiency of (a,b) *E. coli* and *S. aureus* under simulated light. (c,d) *E. coli* and *S. aureus* exposed to sunlight for 10 min by Ag<sub>9</sub>(SiO<sub>4</sub>)<sub>2</sub>NO<sub>3</sub>.

The survival rate vs. time was investigated at low doses of 2  $\mu\text{g}/\text{mL}$ . For each kind of bacterium, the survival rate under simulated and natural light showed identical results, as shown in Figure 3. In the first 6 min, 99% of bacteria were killed, and the remaining germs were killed in the next 10 min. The photographs of *E.coli* colonies on an agar plate after photocatalytic bactericidal treatment with  $\text{Ag}_9(\text{SiO}_4)_2\text{NO}_3$  are shown in Figure 4. Bacterial survival was gradually reduced over time until it was completely removed after 10 min.

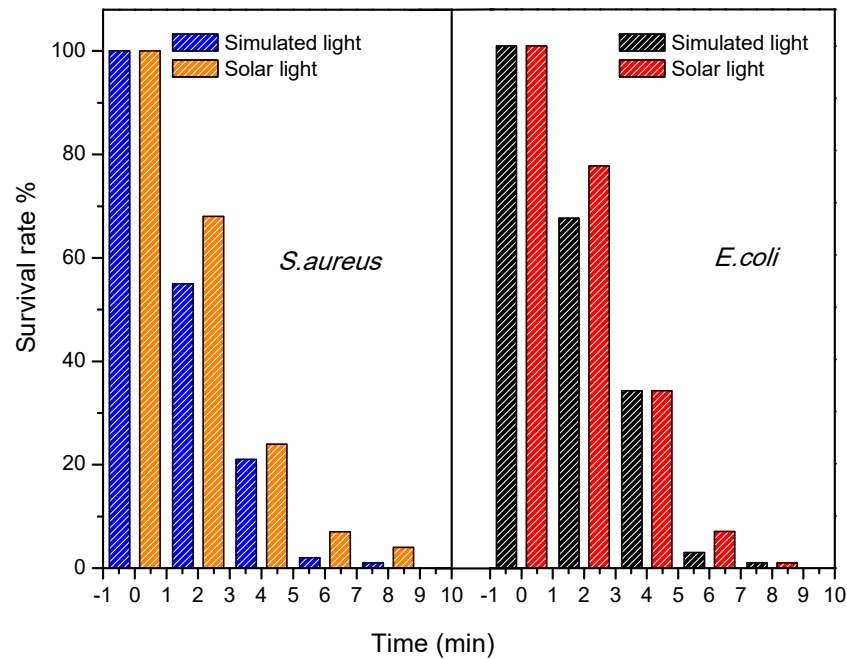


**Figure 3.** Survival rates of *E.coli* and *S.aureus* in the presence of  $\text{Ag}_9(\text{SiO}_4)_2\text{NO}_3$  in simulated and sunlight, respectively.

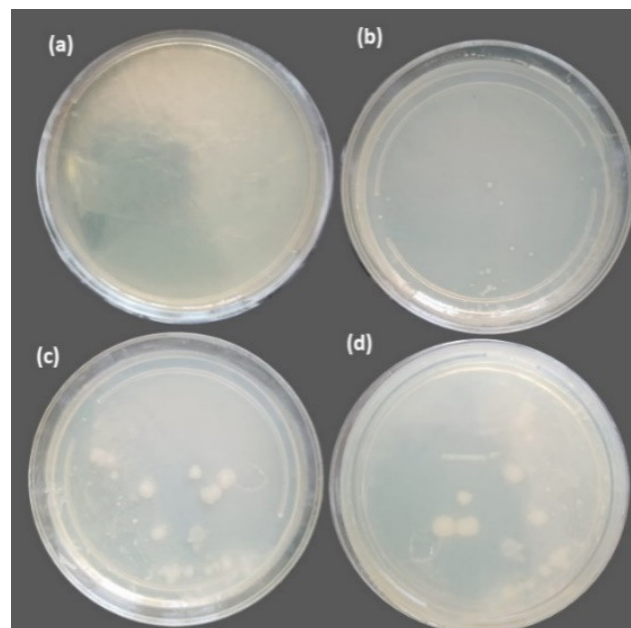


**Figure 4.** Photographs of *E.coli* colonies on an agar plate after photocatalytic bactericidal treatment with  $\text{Ag}_9(\text{SiO}_4)_2\text{NO}_3$  for (a) 10 min, (b) 8 min, (c) 6 min, and (d) 4 min.

According to the results,  $\text{Ag}_9(\text{SiO}_4)_2\text{NO}_3$  demonstrates outstanding bactericidal efficacy. The mechanism of bactericidal efficiency was investigated by including holes and

electron scavenger materials, which play a key role in individually depleting electrons and holes during the photocatalytic operation. Methanol was selected as the hole scavenger and  $\text{AgNO}_3$  was selected as the electron scavenger. Figure 5 demonstrates that the photodegradation of dye was almost completely controlled by holes with little effect from electrons, showing that the oxidation potential is responsible for photodegradation due to  $\text{Ag}_9(\text{SiO}_4)_2\text{NO}_3$  having a deep valence band and a high oxidation potential.

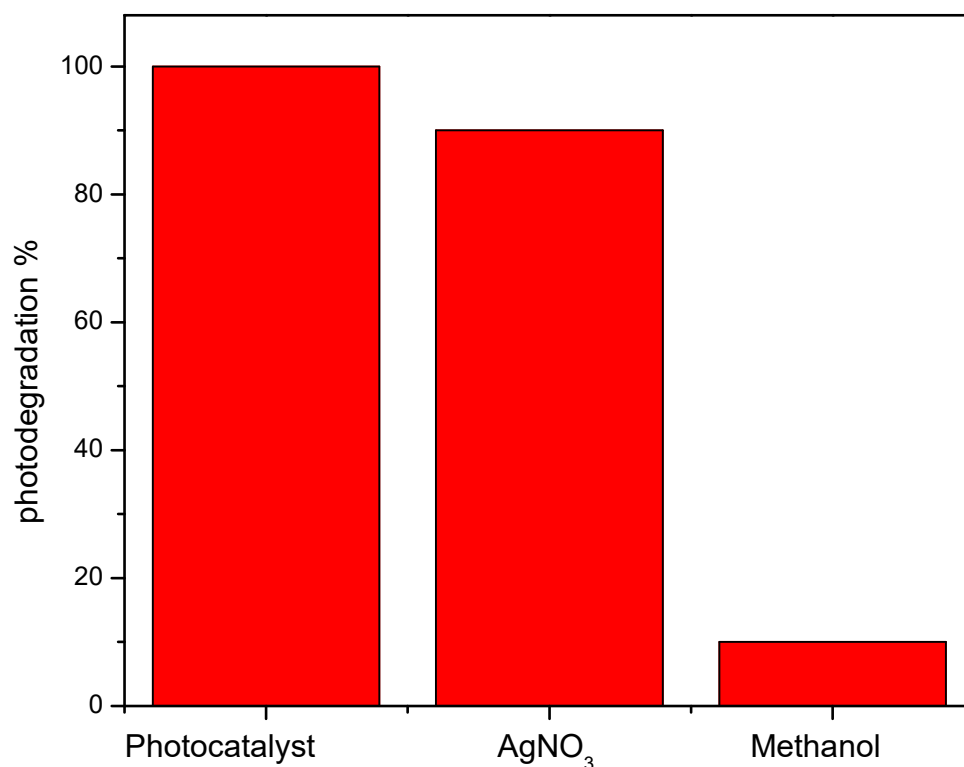


**Figure 5.** Charge carrier trapping experiment,  $\text{AgNO}_3$  as electron scavenger and methanol as hole scavenger of  $\text{Ag}_9(\text{SiO}_4)_2\text{NO}_3$ .

The conduction and valence bands of  $\text{Ag}_9(\text{SiO}_4)_2\text{NO}_3$  were estimated using DFT to confirm that it has high oxidation potential. The conduction and valence bands, respectively, are 0.2 and 1.8 eV vs. a natural hydrogen electrode (NHE). As a result, it is thought that  $\text{Ag}_9(\text{SiO}_4)_2\text{NO}_3$  has high oxidation potential against bacteria, and holes play a key role in its superior bactericidal abilities. Figure 6 shows the proposed photocatalyst band structure and a possible mechanism for photocatalysis reactions based on the DFT simulation. The reactive radicals, particularly the holes produced by the photocatalyst due to the absorbed photon energy, can initiate reduction/oxidation reactions on the membranes of bacterial cells or cause perturbation within the cells, resulting in severe damage, dysfunctional membranes, and ultimately, cell death.

In comparison with previous work, as indicated in Table 1, this work exhibits excellent performance. The photocatalytic bactericidal treatment was performed in the short time (10 min) and at the low concentration of 2  $\mu\text{g}/\text{mL}$ . On the other hand, other silver-based components showed a longer residence period and higher concentrations. The photocatalytic activity of  $\text{Ag}_9(\text{SiO}_4)_2\text{NO}_3$  for dye degradation has been reported to be excellent [28]. Death results because the photocatalyst has a high oxidative potential, capable of destroying the bacterial walls. [28]. The photocatalyst is thought to be an excellent bactericidal option in water or on surfaces.

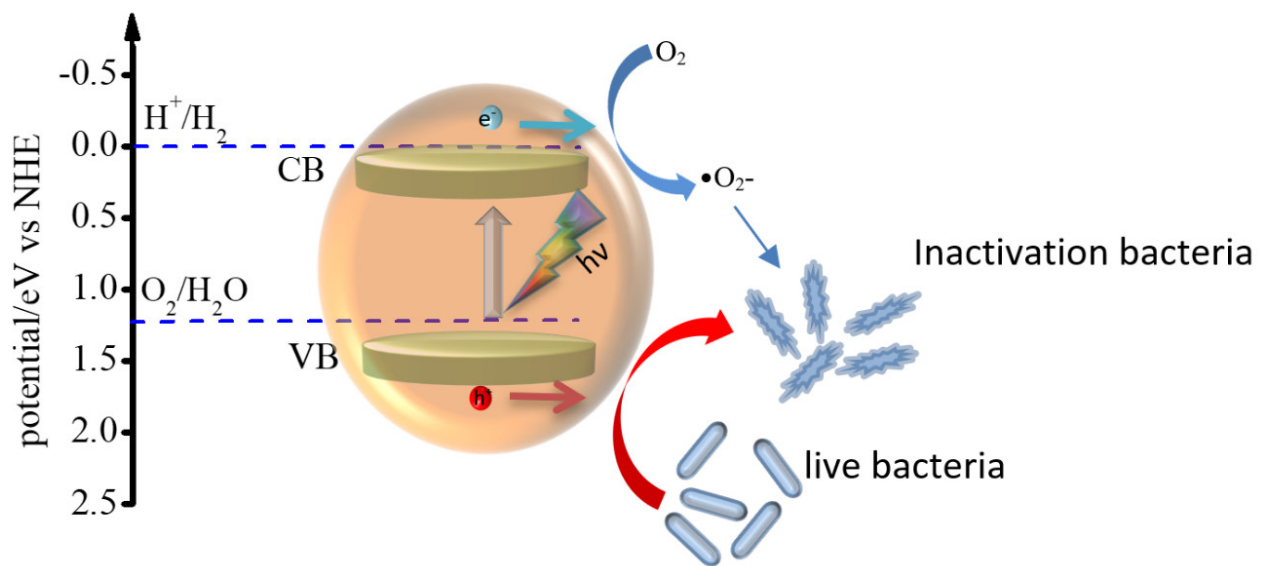


**Figure 6.** The photocatalytic bactericidal mechanism of  $\text{Ag}_9(\text{SiO}_4)_2\text{NO}_3$  under sunlight.

**Table 1.** Comparison of the performance of  $\text{Ag}_9(\text{SiO}_4)_2\text{NO}_3$  with other photocatalysts reported in the literature using (*E. coli*).

Photocatalyst	Initial Concentration ( $\mu\text{g/mL}$ )	Initial Cell Density (cfu/mL)	Final Cell Density (cfu/mL)	Light Source	Time Expose (min)	Ref.
$\text{Ag}_3\text{PO}_4/\text{TiO}_2$	10	$10^{6.2}$	0	Solar light	120	[20]
$\text{Ag}_2\text{O}/\text{TiO}_2$	100	$10^7$	0	300 W Xenon arc lamp, cutoff UV	360	[32]
$\text{Ag}/\text{ZnO}/\text{g-C}_3\text{N}_4$	50	$10^7$	0	300 W Xenon arc lamp, cutoff UV	120	[33]
Ag deposited phosphorus and sulfur co-doped $\text{g-C}_3\text{N}_4$	200	$10^7$	0	300 W Xenon arc lamp, cutoff UV	60	[34]
$\text{Ag}_9(\text{SiO}_4)_2\text{NO}_3$	2	$10^5$	0	Solar light	10	This work

#### 4. Conclusions

In this study, we reported the efficient photocatalytic inactivation of two types of bacteria, Gram-negative (*E. coli*) and Gram-positive (*S. aureus*), under the following two forms of light: solar and simulated light. Under solar light for 10 min, ultra-low concentration of the photocatalyst was found to be 100% bactericidal for both species of bacteria. The photocatalytic mechanism was explored by monitoring the photodegradation of RhB dye, which reveals that holes play a key role in photocatalytic performance. DFT simulations revealed that  $\text{Ag}_9(\text{SiO}_4)_2\text{NO}_3$  has high oxidation potential in the valence bands, which explains the excellent photocatalytic inactivation.

**Author Contributions:** Conceptualization, A.A.-K.; methodology, M.M.T.; formal analysis, R.I.M.; investigation, M.M.T.; data curation, M.A.; writing—original draft preparation, W.H.A.M.; writing—review and editing, W.H.A.M.; supervision, G.F.S.; project administration, A.A.-K.; resources, N.J.A.-B. All authors have read and agreed to the published version of the manuscript.

**Funding:** This work is supported by FRGS FP113-2019A (Malaysian Ministry of Higher Education), Kuala Lumpur, Malaysia.

**Institutional Review Board Statement:** Not applicable.

**Informed Consent Statement:** Not applicable.

**Acknowledgments:** We would like to thank University of Technology-Iraq, Baghdad, Iraq for a support of this work.

**Conflicts of Interest:** The authors declare no conflict of interest.

## References

1. World Health Organization. The Top 10 Causes of Death. 2019. Available online: <https://www.who.int/news-room/fact-sheets/detail/the-top-10-causes-of-death> (accessed on 25 May 2020).
2. Ding, W.; Jin, W.; Cao, S.; Zhou, X.; Wang, C.; Jiang, Q.; Huang, H.; Tu, R.; Han, S.-F.; Wang, Q. Ozone disinfection of chlorine-resistant bacteria in drinking water. *Water Res.* **2019**, *160*, 339–349. [[CrossRef](#)] [[PubMed](#)]
3. Li, D.; Zeng, S.; Gu, A.Z.; He, M.; Shi, H. Inactivation, reactivation and regrowth of indigenous bacteria in reclaimed water after chlorine disinfection of a municipal wastewater treatment plant. *J. Environ. Sci.* **2013**, *25*, 1319–1325. [[CrossRef](#)]
4. Al-Keisy, A.; Mahdi, R.; Ahmed, D.; Al-Attafi, K.; Abd. Majid, W.H. Enhanced Photoreduction Activity in BiOI1-xFx Nanosheet for Efficient Removal of Pollutants from Aqueous Solution. *ChemistrySelect* **2020**, *5*, 9758–9764. [[CrossRef](#)]
5. Mahdi, R.; Alsultan, M.; Al-Keisy, A.; Swiegers, G.F. Photocatalytic Hydrogen Generation from pH-Neutral Water by a Flexible Tri-Component Composite. *Catal. Lett.* **2020**, *151*, 1700–1706. [[CrossRef](#)]
6. Kong, X.; Liu, X.; Zheng, Y.; Chu, P.K.; Zhang, Y.; Wu, S. Graphitic carbon nitride-based materials for photocatalytic antibacterial application. *Mater. Sci. Eng. R Rep.* **2021**, *145*, 100610. [[CrossRef](#)]
7. Christy, A.J.; Suresh, S.; Nehru, L.C. Enhanced antibacterial and photocatalytic activities of nickel oxide nanostructures. *Optik* **2021**, *237*, 166731. [[CrossRef](#)]
8. Zheng, A.L.T.; Sabidi, S.; Ohno, T.; Maeda, T.; Andou, Y. Cu<sub>2</sub>O/TiO<sub>2</sub> decorated on cellulose nanofiber/reduced graphene hydrogel for enhanced photocatalytic activity and its antibacterial applications. *Chemosphere* **2022**, *286*, 131731. [[CrossRef](#)] [[PubMed](#)]
9. Liu, B.; Han, X.; Mu, L.; Zhang, J.; Shi, H. TiO<sub>2</sub> nanospheres/AgVO<sub>3</sub> quantum dots composite with enhanced visible light photocatalytic antibacterial activity. *Mater. Lett.* **2019**, *253*, 148–151. [[CrossRef](#)]
10. Liu, B.; Mu, L.; Han, B.; Zhang, J.; Shi, H. Fabrication of TiO<sub>2</sub>/Ag<sub>2</sub>O heterostructure with enhanced photocatalytic and antibacterial activities under visible light irradiation. *Appl. Surf. Sci.* **2017**, *396*, 1596–1603. [[CrossRef](#)]
11. Qin, Y.; Guo, Y.; Liang, Z.; Xue, Y.; Zhang, X.; Yang, L.; Tian, J. Au nanorods decorated TiO<sub>2</sub> nanobelts with enhanced full solar spectrum photocatalytic antibacterial activity and the sterilization file cabinet application. *Chin. Chem. Lett.* **2021**, *32*, 1523–1526. [[CrossRef](#)]
12. Kavinkumar, V.; Verma, A.; Uma, K.; Moscow, S.; Jothivenkatachalam, K.; Fu, Y.-P. Plasmonic metallic silver induced Bi<sub>2</sub>WO<sub>6</sub>/TiO<sub>2</sub> ternary junction towards the photocatalytic, electrochemical OER/HER, antibacterial and sensing applications. *Appl. Surf. Sci.* **2021**, *569*, 150918. [[CrossRef](#)]
13. Ibrahim, M.A.; Rasheed, B.G.; Mahdi, R.I.; Khazal, T.M.; Omar, M.M.; O'Neill, M. Plasmonic-enhanced photocatalysis reactions using gold nanostructured films. *RSC Adv.* **2020**, *10*, 22324–22330. [[CrossRef](#)]
14. Mahdi, R.; Mohammed, E.H.; Al-Keisy, A.; Alsultan, M.; Majid, W.H.A. Tailoring the morphology of BiNbO<sub>4</sub> of polymorph in 2D nanosheets for enhancement of photocatalytic activity in the visible range. *Phys. E Low-Dimens. Syst. Nanostruct.* **2022**, *136*, 115009. [[CrossRef](#)]
15. Abid, H.N.; Al-keisy, A.; Ahmed, D.S.; Salih, A.T.; Khammas, A. pH dependent synthesis and characterization of bismuth molybdate nanostructure for photocatalysis degradation of organic pollutants. *Environ. Sci. Pollut. Res.* **2022**, 1–11. [[CrossRef](#)] [[PubMed](#)]
16. Wang, Q.; Ji, S.; Li, S.; Zhou, X.; Yin, J.; Liu, P.; Shi, W.; Wu, M.; Shen, L. Electrospinning visible light response Bi<sub>2</sub>MoO<sub>6</sub>/Ag<sub>3</sub>PO<sub>4</sub> composite photocatalytic nanofibers with enhanced photocatalytic and antibacterial activity. *Appl. Surf. Sci.* **2021**, *569*, 150955. [[CrossRef](#)]
17. Zhu, X.; Wang, P.; Huang, B.; Ma, X.; Qin, X.; Zhang, X.; Dai, Y. Synthesis of novel visible light response Ag<sub>10</sub>Si<sub>4</sub>O<sub>13</sub> photocatalyst. *Appl. Catal. B Environ.* **2016**, *199*, 315–322. [[CrossRef](#)]
18. Li, C.; Zhang, Y.; Jin, H.; Kang, W.; Kong, W.; Li, W. Fabrication and visible-light photocatalytic properties of nano-Ag<sub>10</sub>Si<sub>4</sub>O<sub>13</sub>. *Ceram. Int.* **2021**, *47*, 32460–32465. [[CrossRef](#)]
19. Kim, T.-G.; Yeon, D.-H.; Kim, T.; Lee, J.; Im, S.-J. Silver silicates with three-dimensional d<sup>10</sup>-d<sup>10</sup> interactions as visible light active photocatalysts for water oxidation. *Appl. Phys. Lett.* **2013**, *103*, 043904. [[CrossRef](#)]
20. Du, J.; Ma, S.; Yan, Y.; Li, K.; Zhao, F.; Zhou, J. Corn-silk-templated synthesis of TiO<sub>2</sub> nanotube arrays with Ag<sub>3</sub>PO<sub>4</sub> nanoparticles for efficient oxidation of organic pollutants and pathogenic bacteria under solar light. *Colloids Surf. A Physicochem. Eng. Asp.* **2019**, *572*, 237–249. [[CrossRef](#)]
21. Ganguly, P.; Byrne, C.; Breen, A.; Pillai, S.C. Antimicrobial activity of photocatalysts: Fundamentals, mechanisms, kinetics and recent advances. *Appl. Catal. B Environ.* **2018**, *225*, 51–75. [[CrossRef](#)]
22. Karunakaran, C.; Vinayagamoorthy, P. Perforated ZnFe<sub>2</sub>O<sub>4</sub>/ZnO hybrid nanosheets: Enhanced charge-carrier lifetime, photocatalysis, and bacteria inactivation. *Appl. Phys. A* **2017**, *123*, 472. [[CrossRef](#)]
23. Katsumata, H.; Taniguchi, M.; Kaneco, S.; Suzuki, T. Photocatalytic degradation of bisphenol A by Ag<sub>3</sub>PO<sub>4</sub> under visible light. *Catal. Commun.* **2013**, *34*, 30–34. [[CrossRef](#)]



24. Xu, C.; Liu, Y.; Huang, B.; Li, H.; Qin, X.; Zhang, X.; Dai, Y. Preparation, characterization, and photocatalytic properties of silver carbonate. *Appl. Surf. Sci.* **2011**, *257*, 8732–8736. [[CrossRef](#)]
25. Li, J.; Fang, W.; Yu, C.; Zhou, W.; Zhu, L.; Xie, Y. Ag-based semiconductor photocatalysts in environmental purification. *Appl. Surf. Sci.* **2015**, *358*, 46–56. [[CrossRef](#)]
26. Morones, J.R.; Elechiguerra, J.L.; Camacho, A.; Holt, K.; Kouri, J.B.; Ramírez, J.T.; Yacaman, M.J. The bactericidal effect of silver nanoparticles. *Nanotechnology* **2005**, *16*, 2346–2353. [[CrossRef](#)] [[PubMed](#)]
27. Lalueza, P.; Monzón, M.; Arruebo, M.; Santamaría, J. Bactericidal effects of different silver-containing materials. *Mater. Res. Bull.* **2011**, *46*, 2070–2076. [[CrossRef](#)]
28. Liao, C.; Li, Y.; Tjong, S.C. Bactericidal and Cytotoxic Properties of Silver Nanoparticles. *Int. J. Mol. Sci.* **2019**, *20*, 449. [[CrossRef](#)]
29. Al-keisy, A.; Ren, L.; Cui, D.; Xu, Z.; Xu, X.; Su, X.; Hao, W.; Dou, S.X.; Du, Y. A ferroelectric photocatalyst  $\text{Ag}_{10}\text{Si}_4\text{O}_{13}$  with visible-light photooxidation properties. *J. Mater. Chem. A* **2016**, *4*, 10992–10999. [[CrossRef](#)]
30. Zhu, X.; Wang, Z.; Huang, B.; Wei, W.; Dai, Y.; Zhang, X.; Qin, X. Synthesis of  $\text{Ag}_9(\text{SiO}_4)_2\text{NO}_3$  through a reactive flux method and its visible-light photocatalytic performances. *APL Mater.* **2015**, *3*, 104413. [[CrossRef](#)]
31. Clark, S.J.; Segall, M.D.; Pickard, C.J.; Hasnip, P.J.; Probert, M.I.; Refson, K.; Payne, M.C. First principles methods using CASTEP. *Z. Krist.-Cryst. Mater.* **2005**, *220*, 567–570. [[CrossRef](#)]
32. Jin, Y.; Dai, Z.; Liu, F.; Kim, H.; Tong, M.; Hou, Y. Bactericidal mechanisms of  $\text{Ag}_2\text{O}/\text{TNBs}$  under both dark and light conditions. *Water Res.* **2013**, *47*, 1837–1847. [[CrossRef](#)] [[PubMed](#)]
33. Ma, S.; Zhan, S.; Xia, Y.; Wang, P.; Hou, Q.; Zhou, Q. Enhanced photocatalytic bactericidal performance and mechanism with novel  $\text{Ag}/\text{ZnO}/\text{g-C}_3\text{N}_4$  composite under visible light. *Catal. Today* **2019**, *330*, 179–188. [[CrossRef](#)]
34. Xu, X.; Wang, S.; Yu, X.; Dawa, J.; Gui, D.; Tang, R. Biosynthesis of Ag deposited phosphorus and sulfur co-doped  $\text{g-C}_3\text{N}_4$  with enhanced photocatalytic inactivation performance under visible light. *Appl. Surf. Sci.* **2020**, *501*, 144245. [[CrossRef](#)]